Understanding the high neutralization yields in collisions of keV Li^+ ions with copper surfaces

C. Meyer,[1] F. Bonetto,[1,2] R. Vidal,[1,3] Evelina A. García,[1] C. Gonzalez,[4] J. Ferrón,[1,2] and E. C. Goldberg[1,2]

[1]*Instituto de Desarrollo Tecnológico para la Industria Química (INTEC), Consejo Nacional de Investigaciones Científicas y Técnicas (CONICET), Güemes 3450, S3000GLN Santa Fe, Argentina*

[2]*Departamento de Materiales, Facultad de Ingeniería Química, Universidad Nacional del Litoral, Santiago del Estero 2829, S3000AOM Santa Fe, Argentina*

[3]*Departamento de Física, Facultad de Ingeniería Química, Universidad Nacional del Litoral, Santiago del Estero 2829, S3000AOM Santa Fe, Argentina*

[4]*Departamento de Superficies y Recubrimientos, Instituto de Ciencia de Materiales de Madrid (CSIC), ES-28049 Madrid, Spain*

(Received 27 April 2012; revised manuscript received 2 August 2012; published 17 September 2012)

Measurements of neutral atom fractions for Li^+ scattered by Cu(111) and Cu(001) surfaces as a function of the exit ion energy and exit angle are reported. Large neutralization rates (between 20% and 60%) are found in all cases. A first-principles quantum-mechanical based theoretical formalism is applied to describe the time-dependent scattering process, where neutralization to the Li ground state is considered as the unique relevant charge transfer channel during the collision. The increase of the neutralization fraction as the exit energy decreases is well described by the model. The proximity of the projectile energy level to the solid Fermi level and the large extension of the ion-surface coupling interactions, affecting a large number of surface atoms, play a decisive role in explaining the experimental yields.

DOI: 10.1103/PhysRevA.86.032901 PACS number(s): 79.20.Rf, 68.49.Sf, 34.70.+e

I. INTRODUCTION

Charge transfer between an atom (ion) and a surface is a very complex phenomenon whose implications extend over a large number of different fields, going from chemical reactions (as in catalysis, for instance) to electron emission and surface characterization [1,2]. Auger neutralization (AN) and resonant neutralization (RN) are among the most significant mechanisms involved in charge transfer. In AN [3], probably the most efficient neutralization mechanism in ion-surface collisions, the Coulomb repulsion between two electrons in the solid promotes the neutralization of the incoming ion by one of these electrons and the energy promotion of the other one. In RN the neutralization takes place when one electron of the solid tunnels to a projectile energy level that lies within the occupied solid band, i.e., no energy transfer is involved.

Charge exchange is the key process in low-energy ion scattering (LEIS), one of the most widely used surface characterization techniques [4]. As LEIS is based in the detection of scattered ions, to get a good sensitivity surface technique high ion yields at the detector are needed. This situation can be favored by working with projectiles whose ionization level lies close to the sample work function, lowering in this way the probability of neutralization. The alkali-metal ions fill this condition. Since LEIS also needs low-mass projectiles, in order to have a large backscattering probability, Li ions are the best choice for analytical purposes.

As the Li^+ ion approaches the surface, the 2*s* valence level is broadened and shifted upwards due to the image potential effect. This shift will set the Li(2*s*) level above the Fermi level. In this standard picture, neither AN nor RN are expected. However, this simplistic picture of the charge exchange process usually fails. Yarmoff *et al*. showed that the resonant charge transfer (RCT) plays a crucial role in the neutralization of Li^+ ions with several surfaces (Ref. [5] and references therein). They also showed that neutralization of alkali-metal ions is sensitive to the electronic states close to the surface Fermi level. Kimmel *et al*. [6,7] studied the neutralization process of low-energy (5–1600 eV) alkali projectiles on Cu(001), and they showed the relevance of the atomic resonances near the surface for the RCT process. They reported large neutral fractions in Li-Cu(001) collisions (in their scattering geometry the incident and exit angles are equal). The neutral fraction was found to monotonically decrease as the perpendicular velocity increases (the perpendicular energy varies between 4 and 300 eV).

Recently, an unexpectedly large and face-dependent neutralization probability has also been found for Li^+ impinging on the surface of some noble metals (Cu, Ag, and Au) by Esaulov's group [8–11]. They used an experimental setup with an exit angle of 90° and found a nonmonotonic behavior of the neutralization probability, increasing at high and low incident energies. In addition, strong differences between the faces (001) and (111) of Cu were also reported. Since this last result cannot be described by the jellium model, they suggested that the lower neutralization probability for the (111) surface could be explained in terms of a dynamical nonresonant electron transfer involving surface states. In a recent paper [12], presenting results of Li^+ neutralization on Ag-Au(111), Au(110), and Pd(100), the generality of the nonmonotonic dependence of the neutral fraction with incident energy is demonstrated. On the other hand, a nonmonotonic behavior of the neutralization probability with the exit angle is also found.

From the theoretical point of view the field has also been quite active. Different quantum-mechanical approaches were used to describe the charge transfer process in the interaction of Li and metallic surfaces [7,13–18]. Since the pioneering works of Newns and Muda [19,20], several improvements to the time-dependent Anderson Hamiltonian were introduced. For instance, the inclusion of a detailed treatment of the localized and extended characteristics of the projectile-surface interaction results in a clear improvement of the agreement with experimental results [18,21]. In a previous work [21],

we employed the bond-pair approach [22] to describe the neutralization rates observed in Li^+-Cu(111) and Cu(001) collisions. While for high exit energies the model satisfactorily describes the experimental results, it fails to explain the measured neutralization rates for low exit energies.

In this work we present measurements of the neutralization probability of keV Li^+ ions incident along the main crystallographic directions of the Cu(001) and Cu(111) surfaces for different energies and incident angles. We also extended the ion energy range measured by Esaulov and co-workers [8–10] using an experimental setup that allows us to determine the effect of the parallel velocity. From the theoretical point of view, we improved our model by modifying three main features: (i) the crossed elements of the density matrix between different atomic sites of the solid were incorporated in the calculation; (ii) more surface atoms (up to fourth-nearest neighbors) were considered in the collision; and (iii) a symmetrically orthonormalized atomic basis set for the substrate atoms was introduced. The comparison between our experimental results and theoretical calculation allows us to improve our understanding of this quite exciting system.

II. METHODS

A. Theoretical model

Here, the calculation model of Ref. [21] was used to describe the resonant neutralization of Li^+ impinging on Cu(001) and Cu(111). It is assumed that the Li ground state is the only active neutralization channel. To consider or not the spin fluctuation statistic was found not to lead to very different results [18,21]. Thus, the charge transfer process analyzed is focused on the charge fluctuation $Li^+(1s^2) \leftrightarrow Li^0(1s^2 2s)$, neglecting the spin (spinless approximation).

Briefly, an Anderson-like Hamiltonian is used to describe the system under consideration:

$$H = \sum_k \varepsilon_k \hat{n}_k + \varepsilon_a \hat{n}_a + \sum_k [V_{k,a} c_k^+ c_a + \text{H.c.}]. \qquad (1)$$

Here, k corresponds to the surface states, ε_k is the corresponding energy, $\hat{n}_k = \hat{c}_k^+ \hat{c}_k$ is the occupation number; a refers to the projectile active state ($2s$) with energy ε_a and occupancy n_a. Finally, within the *bond-pair* model used [22], $V_{k,a}$ represents the coupling (hopping) between the surface k states and the Li atom $2s$ state. An adiabatic atom-surface interaction is assumed to obtain the hopping terms and the atom energy. A linear combination of atomic orbitals (LCAO) is used to describe the solid k states $\varphi_k = \sum_{i,R_s} c^k_{i,R_s} \phi_i(r - R_s)$ where the coefficients c^k_{i,R_s} are related to the elements of the density matrix through $\rho_{i,j,R_s,R_{s'}}(\varepsilon) = \sum_k c^{k*}_{i,R_s} c^k_{j,R_{s'}} \delta(\varepsilon - \varepsilon_k)$. Here lies the first main difference with the calculation performed in Ref. [21]. In that previous work, the density matrix elements with $\vec{R}_s \neq \vec{R}_{s'}$ were neglected. The FIREBALL code [23,24] was used to calculate $\rho_{i,j,R_s,R_{s'}}(\varepsilon)$ for both Cu surfaces. This code is based on the local-orbital density functional theory.

The coupling term present in Eq. (1) is calculated by using a LCAO expansion given by $V_{k,2s} = \sum_{i,R_s} c^k_{i,R_s} V^{\text{dim}}_{i R_s,2s}$. Here $V^{\text{dim}}_{i R_s,2s}$ includes the two-electron contributions of the dimer projectile-surface atom (at $\vec{R}_s$) under a mean-field approximation. A good atomic basis set for both elements, Li and Cu, is necessary to perform this calculation [25,26]. A relevant difference with the model calculation used in Ref. [21] is the symmetric orthogonal basis set [27] used to describe the states of the surface atoms, in order to be consistent with the calculation of the density matrix [28].

The long range interactions are introduced by considering the image potential. For large normal distances (z), this potential represents an important contribution to the projectile energy level [22,29]:

$$\varepsilon_I(R) = \begin{cases} \tilde{\varepsilon}_I(R) + V_{\text{im}}(z_a) & \text{for} \quad z \leqslant z_a \\ \tilde{\varepsilon}_I(R) + V_{\text{im}}(z) & \text{for} \quad z > z_a \end{cases}$$

$$\text{where} \quad V_{\text{im}}(z) = \frac{1}{4(z - z_{\text{im}})}. \qquad (2)$$

Here, the image plane position z_{im} is assumed to be half of the interlayer distance: 1.71 and 1.97 a.u. for Cu(001) and Cu(111) surfaces, respectively [30]. In addition, $z_a = 8$ a.u. is chosen to match the long range contribution of the image potential [22,29] to the short range contribution of the mean-field model calculation.

To solve the time evolution of the scattering process introduced by the time dependence of the projectile position respect to the surface $R = R(t)$, we use the Green-Keldysh formalism [31]. The average value $\langle \hat{n}_a(t) \rangle$ gives the probability that the projectile state is occupied at the time t. This value is obtained from the Green's function $F_{aa}(t,t') = i \langle \hat{c}_a^+(t') \hat{c}_a(t) - \hat{c}_a(t) \hat{c}_a^+(t') \rangle$, as $\langle \hat{n}_a(t) \rangle = \frac{1}{2}[1 - i F_{aa}(t,t)]$.

In this form, the $F_{aa}(t,t')$ Green's function and the advanced one,

$$G_{aa}(t,t') = i \Theta(t' - t) \langle \hat{c}_a^+(t') \hat{c}_a(t) + \hat{c}_a(t) \hat{c}_a^+(t') \rangle,$$

are necessary to solve the problem. The self-energies determining the motion equations of these Green's functions depend on the local density of the states (Cu DOS) and the atomic Li-Cu hopping integrals through the LCAO expansion of the k states in the $V_{k,2s}$ expression [21].

It is relevant to remark that the theoretical results were obtained assuming a normal trajectory with the corresponding normal component of the incoming kinetic energy (according to the following experimental geometry: incoming angle 45° and exit angle 90°). In other words, in our model we consider a virtual ion moving perpendicularly to the surface all the time (approaching and leaving the surface); with incoming and outgoing velocities identical to the perpendicular components of the speed of a projectile following the experimental geometry. The kinematic factor, i.e., the energy loss factor for the classical binary collision, was also taken into account in the calculation of the outgoing velocities. It is important to point out that in our theoretical model the azimuthal direction of the projectile is irrelevant so experimental results obtained with different azimuths will be contrasted with our calculations.

The number of surface atoms considered in the present work constitutes a remarkable improvement relative to the calculation implemented in Ref. [21]. In this previous work, only the first-nearest neighbors restricted to the first surface layer were considered. In this way, solely seven (five) atoms were taken into account to describe the charge transfer process involved in the collision of Li ions with the Cu(111) [Cu(001)] faces. In the work we are reporting here, the calculation code

was specially prepared to work with a large number of surface atoms. In this way, up to fourth-nearest neighbors and three atomic layers were considered (about 10 a.u. away from the scatter atom). Thus, 37 (34) atoms were involved in the Li-Cu(111) [Cu(001)] charge transfer calculation: 19 (13) atoms from the first atomic layer, 12 (12) atoms from the second atomic layer, and six (nine) atoms from the third atomic layer. The dependence of the present calculation with the number of surface atoms considered is also analyzed.

B. Experimental setup

The experiments were performed in a low-energy ion scattering (LEIS) system that basically consists of an ultrahigh vacuum (UHV) chamber (base pressure in the 10^{-9} mbar range), a differentially pumped ion gun with a velocity filter, and a time-of-flight (TOF) spectrometer. The UHV chamber is also equipped with a low-energy electron diffraction (LEED) system. The Li^+ ions were produced in a discharge source (Colutron) from a heated quartz tube filled with LiCl; then the accelerated beam was mass analyzed using a Wien filter. For LEIS-TOF measurements the ion beam is rapidly swept by applying a square-wave voltage to a pair of deflection plates (chopper plates) located in front of a rectangular slit to produce a pulsed ion beam. The Cu single crystals are then bombarded by this pulsed ion beam.

The energy distributions of the Li^+ ion and Li atom scattered off the sample surface were detected by time-of-flight methods [32,33]. Basically, the trigger output of the deflection plates pulse generator is used as the start pulse for a fast multichannel scaler (Ortec, Microchannel Scaler-MCS). Every particle reaching the detector after being scattered by the sample generates a pulse that is accumulated in a particular time channel of the MCS. After a specific acquisition time the MCS yields a histogram of the distribution of particle flight times (TOF spectrum). The pulse repetition rate was 3 kHz. The scattering angles were fixed at $\theta = 45^\circ$ (forward scattering, FS) and $\theta = 135^\circ$ (backward scattering, BS). In the first case the incoming and exit angles, measured with respect to the surface plane, were varied between 10° and 35°. For BS the exit angle was fixed at 90° and this experimental condition exactly corresponds to the collision geometry assumed in the theoretical model.

To separate the ions from the neutrals, after scattering from the surface, we use a pair of deflection plates placed at the entrance of each drift tube. In FS scattered particles were detected by two microchannel plates (MCP) mounted in a chevron configuration at the end of the drift tube (the sample-to-detector flight path was 155 cm). In BS, scattered particles were detected by a channeltron electron multiplier (CEM) mounted at the end of the drift tube (the sample-to-detector flight path was 137 cm).

The Cu single crystals were mounted on a manipulator that allows changing the incident (α), exit (β), and the azimuthal angles (φ). Clean Cu(001) and Cu(111) surfaces were prepared by repeating cycles of 2-keV Ar^+ small-angle bombardment (20° from the surface) and annealing at 500 °C for 5 min. The cleanliness was checked by TOF-DRS (direct recoil spectroscopy), and the order and orientation of the single crystals were checked by LEED.

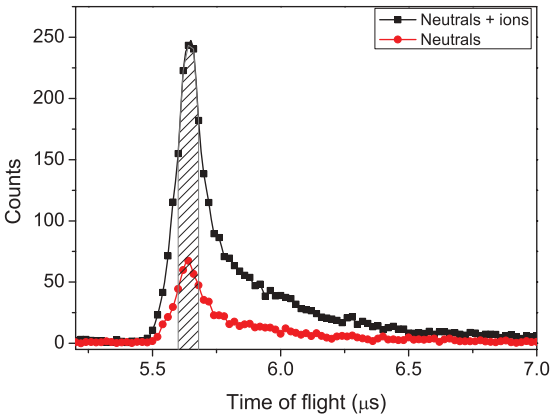

FIG. 1. (Color online) TOF-LEIS spectra of total scattered ions plus neutrals (full squares) and neutral (full circles) particles for $\alpha/\beta = 25^\circ/20^\circ$ (FS), Cu(111), $\varphi = [\bar{1}10]$ and for 3 keV Li^+ incoming energy. The striped area indicates the elastic peak width considered for neutral fraction calculation.

In Fig. 1 we show a typical TOF spectra of total scattered (ions plus neutrals) and neutral particles for 3-keV incident Li^+ ions on Cu(111) at FS and 20° exit angle, from the surface. In both spectra, the elastic peak due to a binary collision of the incoming Li^+ with one surface copper atom is apparent. For larger times of flight there is a broad background due to particles that have penetrated below the surface layer and have scattered from subsurface copper atoms. In these multiple collisions the projectiles are involved in several electron exchange neutralization and reionization processes. Since we are only interested in processes involving binary collisions, the experimental neutral fraction is obtained through the integration of a narrow TOF interval (80 ns, $\Delta E \sim 130$ eV, striped region in the figure) centered at the elastic peak.

III. RESULTS AND DISCUSSION

The experimental setup in LEIS experiments, with a fixed scattering angle, forces us to make a careful analysis of the different variables. Thus, changing the incoming projectile energy, for instance, is associated with changes in parallel and perpendicular velocities of both incoming and scattered ions and atoms. In the same way, changing the (incoming) exit angle for a fixed energy produces the same effect. Since usually, theoretical models deal only with perpendicular velocities, and most of the time they are limited to only exit trajectories, it is important to estimate the limits of such assumptions. Let us first analyze the importance of the incoming trajectory.

In order to analyze the importance of the incoming trajectory we performed the following experiment. Using the backward scattering setup (scattering angle equal to 135°), we changed the incoming energy and incident and/or exit angles in order to have large variations of the incoming perpendicular energy while keeping constant the perpendicular exit energy. We varied the incident angle between 30° and 60°, and at the same time the exit angle changed between 105° and 75°. As the exit angle changed only $\pm 15^\circ$ around the normal direction the exit parallel energy is almost the same (close to zero), but the incident parallel energy change was large (it varied between 800 and 2400 eV). In Fig. 2 we show that, under these

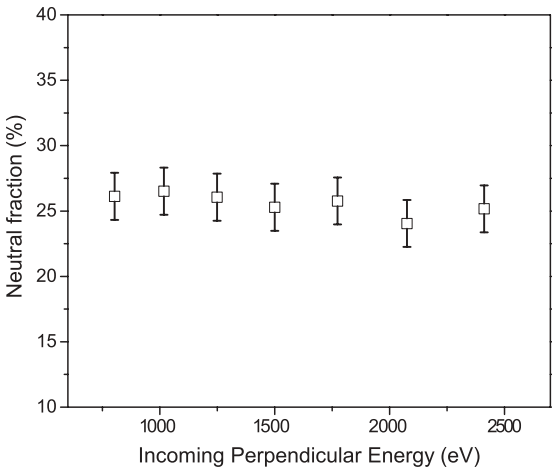

FIG. 2. Neutral fraction as a function of the incoming perpendicular energy $E_i = E_0\cos^2(\alpha)$ for Li^+ incident on Cu(111) in backscattering. The perpendicular exit energy was kept constant at 2064 eV (see text).

conditions, the neutralization probability is constant. This fact lead us to a very important conclusion: The final charge state of the scattered projectiles is completely determined along the exit trajectory, validating the usual assumption made in theoretical models.

Since in this experiment we wanted to isolate the incoming trajectory effects, we kept constant the exit perpendicular velocity and allowed only minor variations of the parallel one. Thus, we cannot assure with this evidence that the only important physical parameter in these experiments is the exit perpendicular velocity. We will later show that this is not the case.

In Fig. 3 we show our experimental results of the neutral fraction as a function of the perpendicular exit velocity for Li^+ impinging on Cu(001), compared with our theoretical predictions for the same face. Since different azimuthal angles (not considered in the theory) as well as different exit energies and parallel velocities are depicted together, with perpendicular velocity as the only parameter, the analysis must be carefully done. Experimental results of Kravchuk *et al.* [9] are included for comparison.

In agreement with previous reports [8–10] we found a quite large neutral fraction compared with our expectations based on a simple picture of the location of the Li ground state relative to the Fermi level. We also found a strong dependence with the perpendicular energy (velocity) for low energies, as well as for the different azimuths. As the perpendicular energy increases the dependence of the neutral fraction with energy and azimuth disappears and the neutralization probability tends to a nearly constant value. This result is clearly consistent with the theoretical predictions. The strong increase of the neutral fraction for small energies, also reported by Kravchuk *et al.*, is reproduced by our calculation, although in a smoother way.

The remarkable dependence on the azimuthal angle is clear evidence of the extension of the Li-Cu interaction. Due to this interaction, the inclusion of the ion trajectory seems to be mandatory in any model that includes the lowest energies. Our model shows a better agreement with the [110] azimuthal directions than with the less compact [100]. When considering the ion trajectory, it seems reasonable that compact directions have more effect on the grazing exit trajectories (larger parallel velocities), increasing the neutralization probability. However, even when along the [110] direction surface atoms are closer; along the other directions the Li interaction with second-layer atoms may become important. Agreement with results presented in Kravchuk *et al.* [9] mainly occurs for trajectories along the less compact direction, consistent with the fact that their measurements are performed for normal ejection being then less sensitive to the azimuthal direction.

In Fig. 4 we depict our results for the (111) face. We can see that, for the same perpendicular energy, ions with larger energy (5 keV) have systematically larger neutralization probabilities (although differences are small). As the only difference in these experiments is the parallel velocity, this result supports the idea

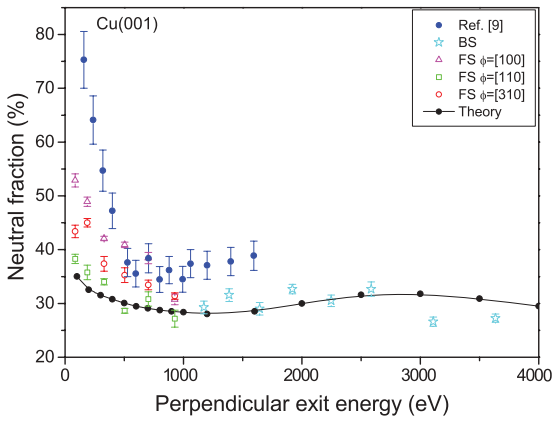

FIG. 3. (Color online) Neutralization probability for Li on Cu(001) as a function of the exit (perpendicular) energy. Experiment: Open symbols correspond to backscattering (BS) results and different azimuthal angles measured in forward scattering (FS). Full blue circles correspond to Ref. [9]. Theoretical results are shown for comparison (full small circles plus solid line).

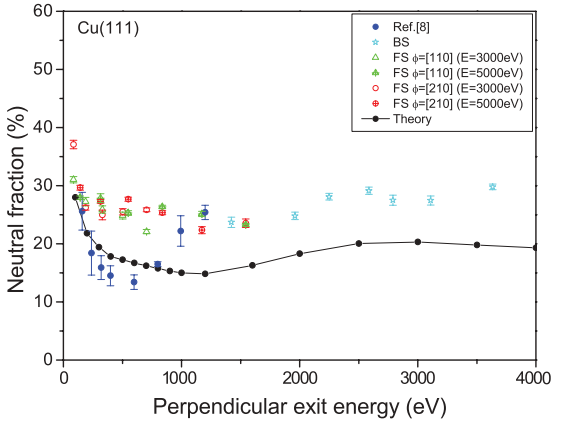

FIG. 4. (Color online) Neutralization probability for Li on Cu(111) as a function of the exit (perpendicular) energy. Experiment: Open symbols correspond to backscattering (BS) results and different azimuthal angles measured in forward scattering (FS) for a couple of exit energies. Full blue circles correspond to experimental results in Ref. [8]. Theoretical results are also shown (full small circles plus solid line).

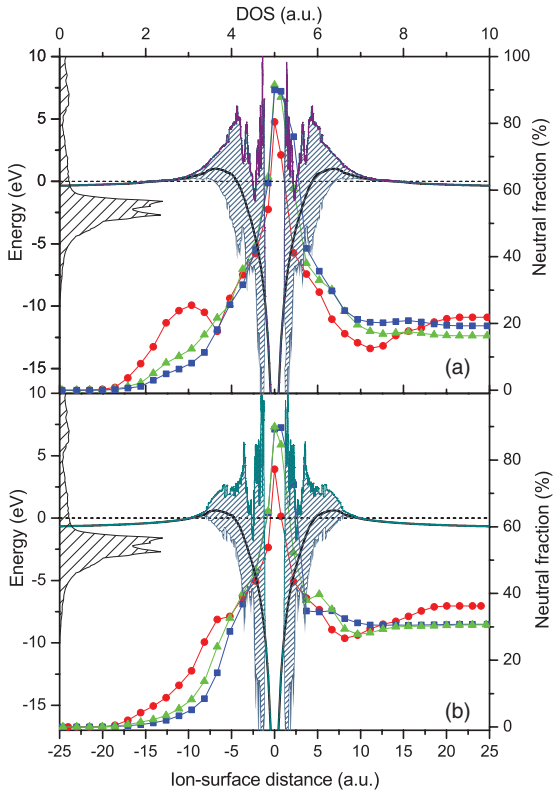

FIG. 5. (Color online) Normal distance dependence of the calculated neutral fraction along the trajectory for Cu(111) [Fig. 5(a)] and Cu(001) [Fig. 5(b)] faces. Three different projectile exit energies (squares, triangles, and circles for 4000, 1600, and 200 eV, respectively) are plotted to appreciate their dissimilar behavior from about 15 a.u. The solid gray line and the connected shadowed region indicate the projectile ionization energy level and its width as a function of z, referred to as the surface Fermi level ($E_{\text{Fermi}} = 0$, dotted line). The Cu total local DOS (striped gray region) is also shown.

that the exit parallel velocity could influence the electronic interaction.

Let us analyze the neutralization probability as a function of the perpendicular velocity. The general qualitative trend is shared for theoretical and experimental results, although important differences are also apparent. The neutralization probability exhibits a minimum in all cases. It significantly increases as the energy decreases, and it slightly grows tending to a saturation value for larger energies. The theoretical and experimental results show clear differences between both crystallographic faces.

Experimentally a minimum is obtained, although when compared to Ref. [8] results, differences in the location and magnitude of such a relative minimum are found. A deeper insight about the different experimental setups used, mainly the exit velocity characteristics, might shed some light on these differences.

The theoretical results predict in both faces an important relative minimum followed by a less pronounced relative maximum. Experimentally, this relative maximum might become visible in the measurements on the (001) face but it is less clear on the (111) face.

Figure 5 shows the theoretical evolution of the projectile neutral fraction plotted as a function of the perpendicular ion-surface distance, z (distance between the projectile and the first atomic layer of the target surface), relative to the turning point. Three different exit energies were considered for both crystallographic faces Cu(111) [Fig. 5(a)] and Cu(001) [Fig. 5(b)]. The total density of states (DOS) of Cu and the evolution of the Li ionization level (solid line) with its adiabatic width calculated as $\Gamma(\varepsilon_a) = 2\pi \sum_k |V_{ak}|^2 \delta(\varepsilon_a - \varepsilon_k)$ (shaded region) along the ion trajectory are also shown in this figure.

Negative distances represent the incoming trajectory. We observe an interesting effect in this part of the trajectory. For Cu(111), the Li ionization level starts below the Fermi level favoring the electron capture and thus, neutralization. However, between 11 and 7 a.u. the projectile energy level and width remain above the Fermi level and electron loss becomes the only mechanism allowed. This effect is clearly observed in the neutralization curve for 200-eV ions where the neutral fraction decreases in this region, but it is not perceived for higher-energy ions. The adiabatic situation is evidently not reached for 1600- and 4000-eV projectiles and, therefore, the neutral fraction is unable to instantaneously "map" the details of the energy level and width. Note that this feature is not present in the Cu(001) and thus, the subsequent neutral fraction decrease is not observed for 200-eV projectiles. For distances closer to 7 a.u., a considerable downshift of the projectile energy level (well below the surface Fermi level) enhances the electron capture and, thus, neutralization. As a consequence, Li ions are mostly neutralized close to the surface, and while the neutral fraction increases with the energy, it tends to saturate for energies close to 1 keV. The projectile-surface distance of maximum approach (turning point) and the time spent by the projectile near the surface appear as the key factors in the neutralization values obtained at the end of the incoming trajectory. Nevertheless, our calculations of an incoming neutral Li atom lead to the same results of the final neutral fractions in the analyzed energy range, clearly demonstrating that the final charge state is defined during the outgoing trajectory.

At the starting point of the outgoing trajectory the projectile atoms are nearly fully neutralized. At this point, and due to the large energy level width product of the strong interaction, the electron loss from the projectile atom turns out to be the most probable charge transfer process. The electron loss is enhanced as the projectile leaves the surface because the projectile energy level gets closer to the solid Fermi level, decreasing in this way the neutralization fraction.

However, a crucial phenomenon arises at the last stage of the outgoing trajectory. At a projectile-surface distance of about 14 (8) a.u. for Cu(111) [Cu(001)], the projectile energy level crosses down the Fermi level (see Fig. 5) making possible the electron capture process. For a negligible energy level width (as it is generally at these distances) the electron capture would not be feasible. However, the extended nature of the Li-Cu system coupling interaction that requires the inclusion of more surface atoms, which slightly but not negligibly contribute to the energy width, makes the electron capture viable at such large distances.

As expected, the process described above becomes more significant as the exit energy decreases. Under a low exit energy picture, the projectile atom has more time to "see"

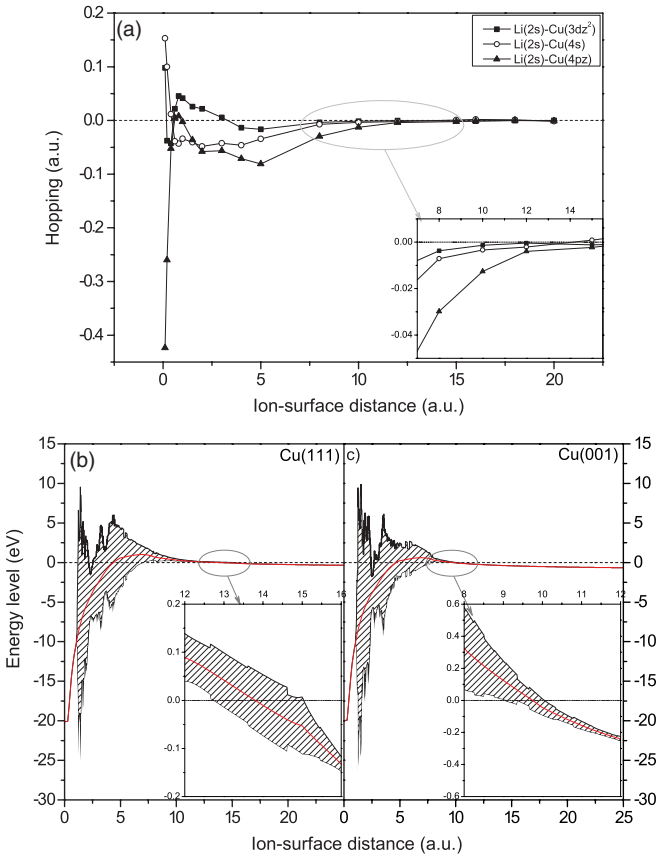

FIG. 6. (Color online) The coupling interaction between the projectile Li(2*s*) state and the scatter surface atom Cu(3*dz*2), Cu(4*s*), and Cu(4*pz*) states are shown as a function of the distance to the surface in Fig. 6(a) [the result is valid for both faces, Cu(111) or Cu(001)]. A still significant hopping term at a distance between 7 and 15 a.u. can be observed in the inset of this figure. This observation strongly suggests the inclusion of surface atoms up to a distance of about 15 a.u. from the central atom. The projectile energy levels and adiabatic width can be observed in Figs. 6(b) and 6(c) for Cu(111) and Cu(001), respectively. In their insets the crossing region is magnified to appreciate the still relevant energy level width.

(through the Li-Cu hopping) the surface atoms, enhancing in this way the electron capture process and provoking the increasing of the neutral fraction at low energies. Note also that the neutralization fraction becomes more sensitive to the crystal structure, leading to larger differences between Cu(111) and Cu(001) neutralization rates at low exit energies.

In Fig. 6(a) we plot the most important hopping terms showing that they are still not zero at the distances considered. In Figs. 6(b) and 6(c), the projectile energy level and width are zoomed in the region where it crosses down the Fermi level. A still significant energy width can be observed in the inset of the figure.

The results depicted in Fig. 6 suggest that we can expect a strong dependence with the perpendicular velocity, a clear dependence with the electronic surface structure (face dependent), and cannot rule out the possibility of a parallel exit velocity effect, mainly due to the extended Li 2*s* state. The comparison with experiments allows us to gain insight about all these points.

The remarkable differences in neutralization values obtained for Cu(111) and Cu(001) are mainly due to the very distinct work functions for both faces: 4.95 and 4.6 eV, respectively. The lower work function of the Cu(001) increases the probability of electron capture from the surface, leading in consequence to a higher neutralization of Li^+ ions.

The presence of the local minimum and maximum observed in both faces is essentially a consequence of a subtle balance between three factors: the energy level position (relative to the Fermi level), the energy level width, and the perpendicular energy considered. As was previously established, the number of atoms considered plays a major role in the determination of the energy level width. In this work we considered up to 37 (34) surfaces atoms for Cu(111) [Cu(001)] surfaces. However, the inclusion of more surface atoms is expected to improve the calculation, especially for very low and very high energies and grazing conditions. According to Fig. 6, the convergence of the neutral fraction with the number of surface atoms would be reached when atoms up to 15 (10) a.u. away from the central point (scatter atom) are included for Cu(111) [Cu(100)]. It implies that considering up to fourth-nearest neighbors would be roughly sufficient to achieve convergence, although a calculation including up to fifth- or sixth-nearest neighbors (not performed in the present work due to the extremely high calculation times involved) is essential to precisely assess it.

In a recent paper [12], the increase in the experimental neutralization observed at low energies was reasonably well described by a simplified description of the collision process. This calculation is based on a linearized rate equation for determining the Li valence electrons as a function of the distance to the surface, using density functional theory (DFT) to describe the Li-surface interaction. By contrast, the present calculation contains a thorough dynamical quantum description of the whole collision process described by a time-dependent Anderson model that allows obtaining neutralization rates at any time point, permitting a more exhaustive analysis of the physical mechanisms linked to the charge transfer process studied. It is also important to mention that the present calculation offers a good description of the different features observed in the experimental neutralization vs energy curves, such as the position of the minimum neutralization magnitude and the general trend observed.

In order to assess how relevant are the different modifications introduced in the theoretical model, in Fig. 7(a) we contrast the Li 2*s* energy level width for Cu(111) obtained from different calculations: (i) Ref. [17]; (ii) Ref. [12]; (iii) our previous calculation Ref. [21], where only the first-nearest neighbors and diagonal terms of the density matrix were taken into account; (iv) our previous calculation improved by considering the crossed terms of the density matrix; and (v) the current calculation including up to fourth-nearest neighbors and the complete density matrix. In Fig. 7(b) we compare the neutral fractions corresponding to cases (ii)–(v).

Considerable differences in neutral fractions are encountered when the present model is contrasted with other models even when the energy level widths are comparable [compare results of Refs. [12,21] in Figs. 7(a) and 7(b)]. It is important to remark that Chen *et al.* [12] assume that the evolution of the number of Li valence electrons can be determined, in a first approximation, from a linearized rate equation. This simplified

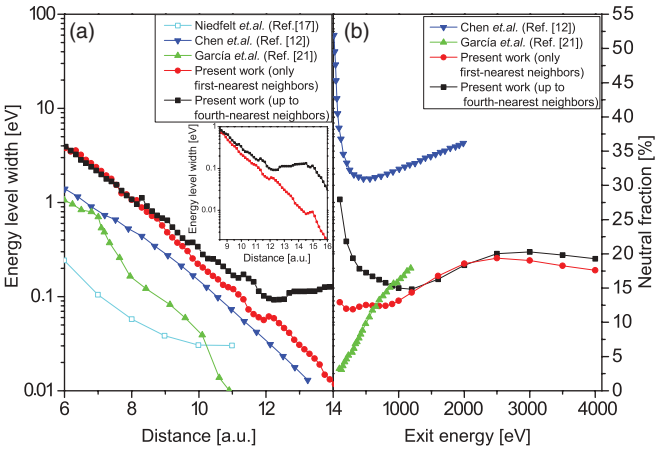

FIG. 7. (Color online) (a) The energy level width for the Li-Cu(111) system is compared for different calculations: (i) Ref. [17]; (ii) Ref. [12]; (iii) our previous calculation, Ref. [21], where only the first-nearest neighbors and diagonal terms of the density matrix were taken into account; (iv) our previous calculation improved by considering the crossed terms of the density matrix; and (v) the current calculation including up to fourth-nearest neighbors and the complete density matrix. The comparison between cases (iv) and (v) is extended up to 16 a.u. to show the appreciable differences at large distances (inset). In (b) the neutral fractions corresponding to cases (ii)–(v) are contrasted.

scheme that links the transition probability with the width of the partial density of states on Li does not take into account the quantum interferences between the transition amplitudes along the projectile trajectory.

The comparison between the present, intermediate, and previous calculations reveals that the inclusion of the density matrix cross-terms introduces a major transformation in the energy level width and in the whole range of the neutral fraction vs energy curve. Alternatively, the insertion of more surface atoms barely alters the energy level width up to around 8 a.u. However, for bigger distances the continuously larger energy level width when more atoms are included [inset, Fig. 7(a)] leads to a substantial increase of the neutral fraction in the low-energy range, consistent with the experimental data (see Fig. 4). Although not shown, similar results were found for Cu(001).

IV. CONCLUSIONS

We report experimental and theoretical results about the neutralization probability of Li^+ ions on Cu(001) and (111) surfaces. In agreement with previous findings, we found an unexpectedly high neutralization probability, based on the simple idea of atom level location and image forces.

We show both experimentally and theoretically that the neutralization probability is completely determined along the exit trajectory. We found a strong dependence on the face (basically due to the different work functions) and also on the azimuthal angle. This allows us to conclude that the extension of the Li 2*s* state, leading to electronic interactions with the substrate for quite large distances, causes the neutralization probability to depend not only on the electronic structure around the scattering center, but also on the electronic structure along the complex trajectory. If we want to analyze cases with parallel velocity, we need to include the exit ion trajectory in our model.

A theoretical formalism was applied to contrast experimental results with calculations. The experimental neutralization vs exit energy general dependence is very well reproduced by the model for both Cu faces, while important differences in magnitudes are observed for Cu(111). A detailed analysis of the neutralization rate evolution allow us to conclude: (i) the final projectile charge state is mostly defined during the outgoing trajectory, being especially relevant the last part of this trajectory (distances higher than 14 a.u.) for low exit energies; (ii) the insertion of the density matrix cross-terms introduces remarkable changes in the energy level widths as well as in the neutralization fraction vs energy curve (whole energy range); (iii) the inclusion of a large number of surface atoms is essential to explain the observed trend of the neutral fraction in the low-energy range; and (iv) the unexpectedly high neutralization observed at low energies can be primarily attributed to the peculiarly large extension of the Li-Cu coupling.

A more accurate description of the Tamm surface state which is pushed out of the top of the *d* band in the case of Cu(111) [34–36], and the inclusion of the Cu(001) image states [37,38] might lead to further improvements in the calculation. The presence of a Tamm state near the Cu(111) surface may introduce relevant modifications in the neutralization at large energies, where short projectile-energy distances are permitted and play a significant role. Alternatively, the image state may become important in Cu(001) due to a possible bonding interaction with the Li 2*s* state (see Ref. [21]).

ACKNOWLEDGMENTS

We would like to thank Dr. Maria Luz Martiarena for very helpful discussions. This work was supported by ANPCyT through PICT Grants No. 14730, No. 14724, and No. 00811; and U.N.L. through CAI + D grants.

[1] J. Los and J. J. C. Geerlings, Phys. Rep. **190**, 133 (1990).
[2] P. Nordlander and J. C. Tully, Phys. Rev. B **42**, 5564 (1990).
[3] H. D. Hagstrum, Phys. Rev. **96**, 336 (1954).
[4] H. Niehus, W. Heiland, and E. Taglauer, Surf. Sci. Rep. **17**, 213 (1993).
[5] J. A. Yarmoff, Y. Yang, G. F. Liu, X. Chen, and Z. Sroubek, Vacuum **73**, 25 (2004).
[6] G. A. Kimmel and B. H. Cooper, Phys. Rev. B **48**, 12164 (1993).
[7] J. B. Marston, D. R. Andersson, E. R. Behringer, B. H. Cooper, C. A. DiRubio, G. A. Kimmel, and C. Richardson, Phys. Rev. B **48**, 7809 (1993).
[8] A. R. Canario, T. Kravchuk, and V. A. Esaulov, New J. Phys. **8**, 227 (2006).

[9] T. Kravchuk, Y. Bandourine, A. Hoffman, and V. A. Esaulov, Surf. Sci. Lett. **600**, L265 (2006).
[10] M. Wiatrowsky, N. Lavagnino, and V. A. Esaulov, Surf. Sci. Lett. **601**, L39 (2007).
[11] H. Hamoudi, C. Dablemont, and V. A. Esaulov, Surf. Sci. **302**, 2486 (2008).
[12] L. Chen, J. Shen, J. Jia, T. Kandasamy, K. Bobrov, L. Guillemot, J. D. Fuhr, M. L. Martiarena, and V. A. Esaulov, Phys. Rev. A **84**, 052901 (2011).
[13] A. G. Borisov, A. K. Kazansky, and J. P. Gauyacq, Surf. Sci. **430**, 165 (1999).
[14] T. Hecht, H. Winter, A. G. Borisov, J. P. Gauyacq, and A. K. Kazansky, Phys. Rev. Lett. **84**, 2517 (2000).
[15] A. G. Borisov, J. P. Gauyacq, E. V. Chulkov, V. M. Silkin, and P. M. Echenique, Phys. Rev. B **65**, 235434 (2002).
[16] K. Niedfeldt, E. A. Carter, and P. Nordlander, J. Chem. Phys. **121**, 3751 (2004).
[17] K. Niedfeldt, P. Nordlander, and E. A. Carter, Phys. Rev. B **74**, 115109 (2006).
[18] F. Bonetto, M. A. Romero, E. A. Garcia, R. A. Vidal, J. Ferrón, and E. C. Goldberg, Phys. Rev. B **78**, 075422 (2008).
[19] D. M. Newns, Phys. Rev. **178**, 1123 (1969).
[20] Y. Muda and D. M. Newns, Phys. Rev. B **37**, 7048 (1988).
[21] E. A. Garcia, M. A. Romero, C. Gonzalez Pascual, and E. C. Goldberg, Surf. Sci. **603**, 597 (2009).
[22] P. G. Bolcatto, E. C. Goldberg, and M. C. G. Passeggi, Phys. Rev. B **58**, 5007 (1998).
[23] J. P. Lewis, K. R. Glaesemann, G. A. Voth, J. Fritsch, A. A. Demkov, J. Ortega, and O. F. Sankey, Phys. Rev. B **64**, 195103 (2001).
[24] P. Jelinek, H. Wang, J. P. Lewis, O. F. Sankey, and J. Ortega, Phys. Rev. B **71**, 235101 (2005).
[25] S. Huzinaga, J. Andzelm, M. Klobukowsky, E. Radzio-Andzelm, Y. Sakai, and H. Tatewaki, *Gaussian Basis Set for Molecular Calculations* (Elsevier, Amsterdam, 1984).
[26] S. Huzinaga, J. Chem. Phys. **42**, 1293 (1965).
[27] P. Löwdin, J. Chem. Phys. **18**, 365 (1950).
[28] M. A. Romero, A. Iglesias-García, and E. C. Goldberg, J. Phys.: Condens. Matter **24**, 045004 (2012).
[29] M. C. Torralba, P. G. Bolcatto, and E. C. Goldberg, Phys. Rev. B **68**, 075406 (2003).
[30] N. V. Smith, C. T. Chen, and M. Weinert, Phys. Rev. B **40**, 7565 (1989).
[31] L. V. Keldysh, Zh. Eksp. Teor. Fiz. **47**, 1515 (1964).
[32] H. H. Brongersma, M. Draxler, M. de Ridder, and P. Bauer, Surf. Sci. Rep. **62**, 63 (2007).
[33] O. Grizzi, M. Shi, H. Bu, and J. W. Rabalais, Rev. Sci. Instrum. **61**, 740 (1990).
[34] A. Gross, *Theoretical Surface Science: A Microscopic Perspective* (Springer-Verlag, Berlin, 2009).
[35] A. Euceda, D. M. Bylander, and L. Kleinman, Phys. Rev. B **28**, 528 (1983).
[36] R. Courths, H. Wern, and S. Hüfner, Solid State Commun. **61**, 257 (1987).
[37] E. V. Chulkov, V. M. Silkin, and P. M. Echenique, Surf. Sci. **437**, 330 (1999).
[38] A. R. Canário, A. G. Borisov, J. P. Gauyacq, and V. A. Esaulov, Phys. Rev. B **71**, 121401 (2005).